

Supplemental material

Gerson-Gurwitz et al., <https://doi.org/10.1083/jcb.201807041>

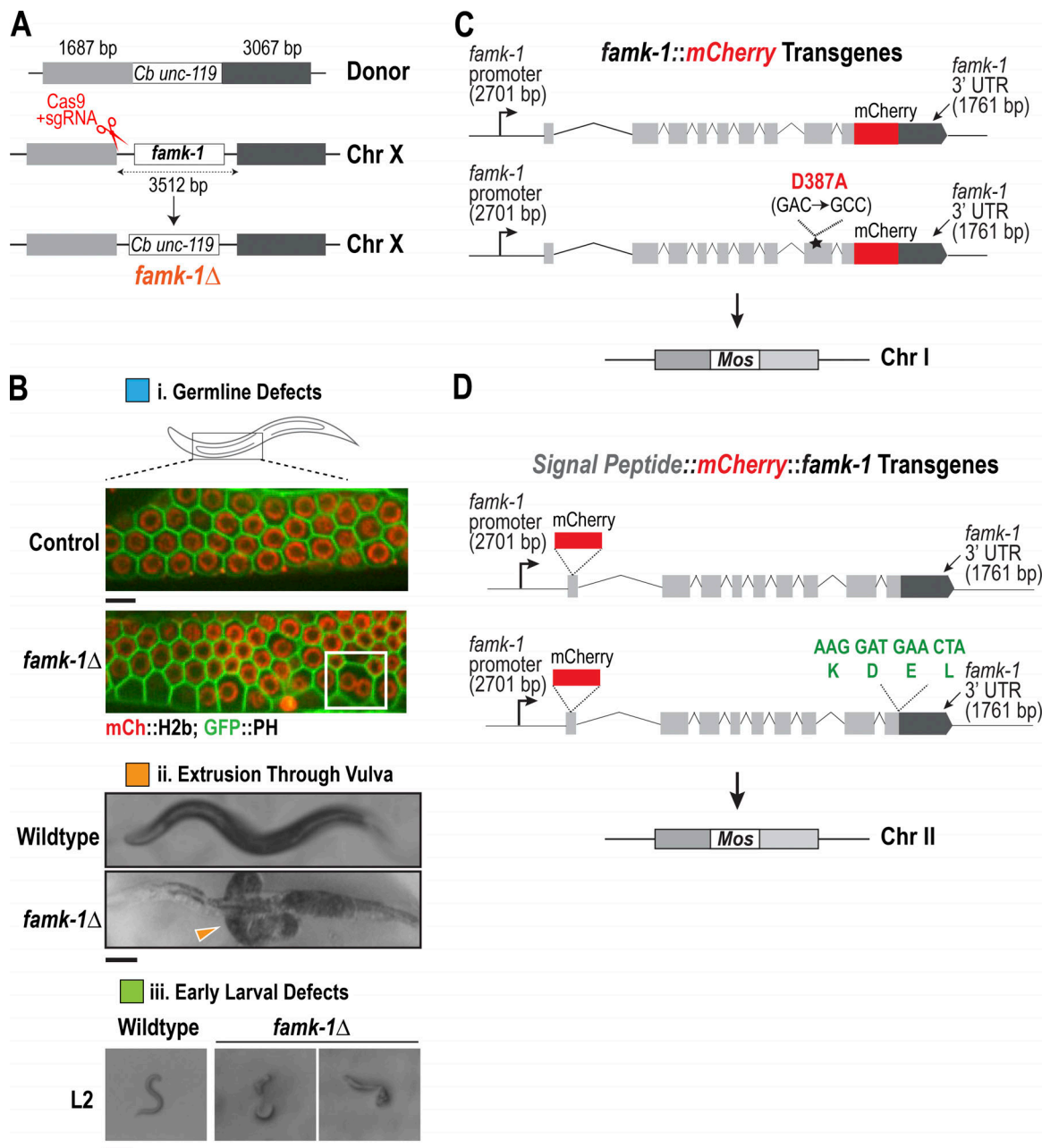


Figure S1. Generation of *famk-1* Δ , *famk-1* single-copy transgenes, and images of phenotypes observed in *famk-1* Δ . (A) Schematic of *famk-1* Δ mutant generation. The entire *famk-1* coding sequence was replaced with the *Cb unc-119* marker. (B) Images of post-hatching defects observed in *famk-1* Δ larvae and adults. Arrowhead points to the extruded intestine. Colored boxes represent phenotypic categories described in Fig. 1 D. Scale bar in B(i), 5 μ m; scale bars in B(ii) and B(iii), 100 μ m. (C) Schematic of *famk-1*::*mCherry* transgene. (D) Schematic of WT and KDEL *mCherry*::*famk-1* transgenes.

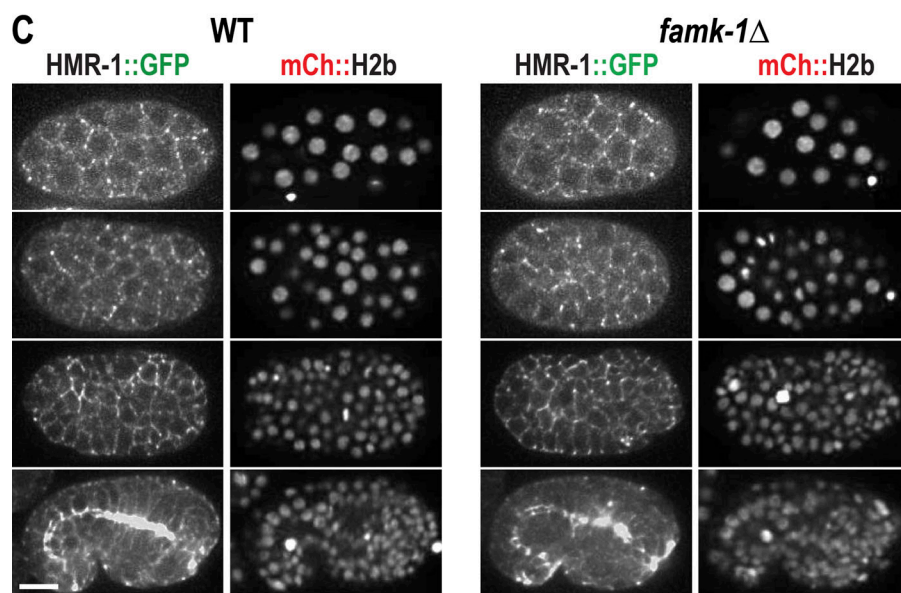
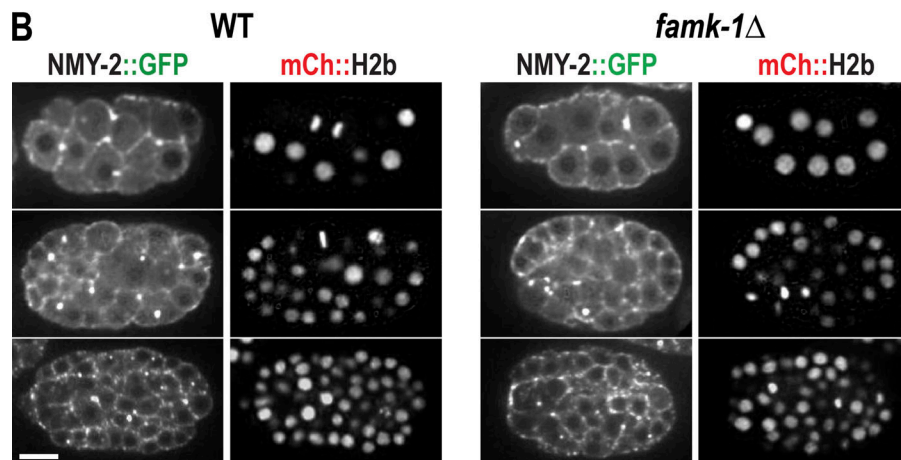
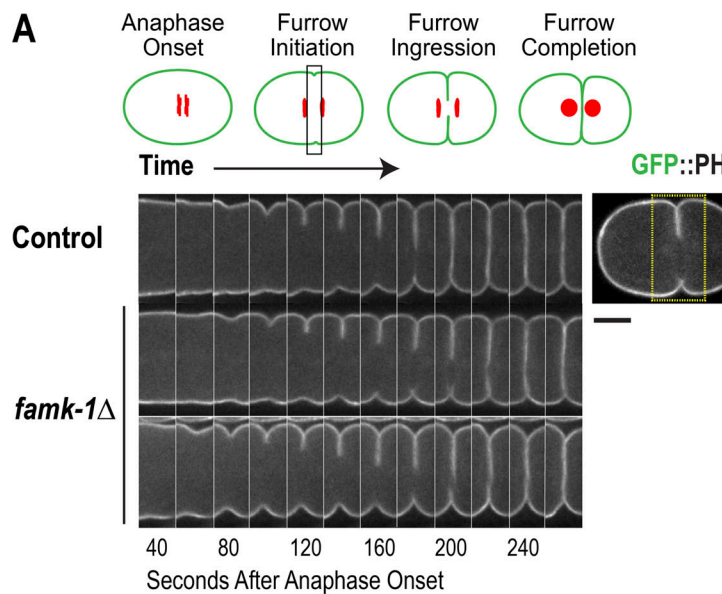


Figure S2. Analysis of cytokinetic furrow ingression and localization of NMY-2 and HMR-1 in *famk-1Δ*. **(A)** One-cell-embryo imaging of control and *famk-1Δ* embryos expressing GFP-fused plasma membrane marker. Similar results were observed in 10 imaged control and *famk-1Δ* embryos. Scale bar, 10 μm. **(B and C)** Localization of NMY-2::GFP (B) and HMR-1::GFP (C) at different-stage control and *famk-1Δ* embryos. No obvious localization differences were evident for either NMY-2 or HMR-1 between control and *famk-1Δ* embryos. Scale bars, 5 μm.

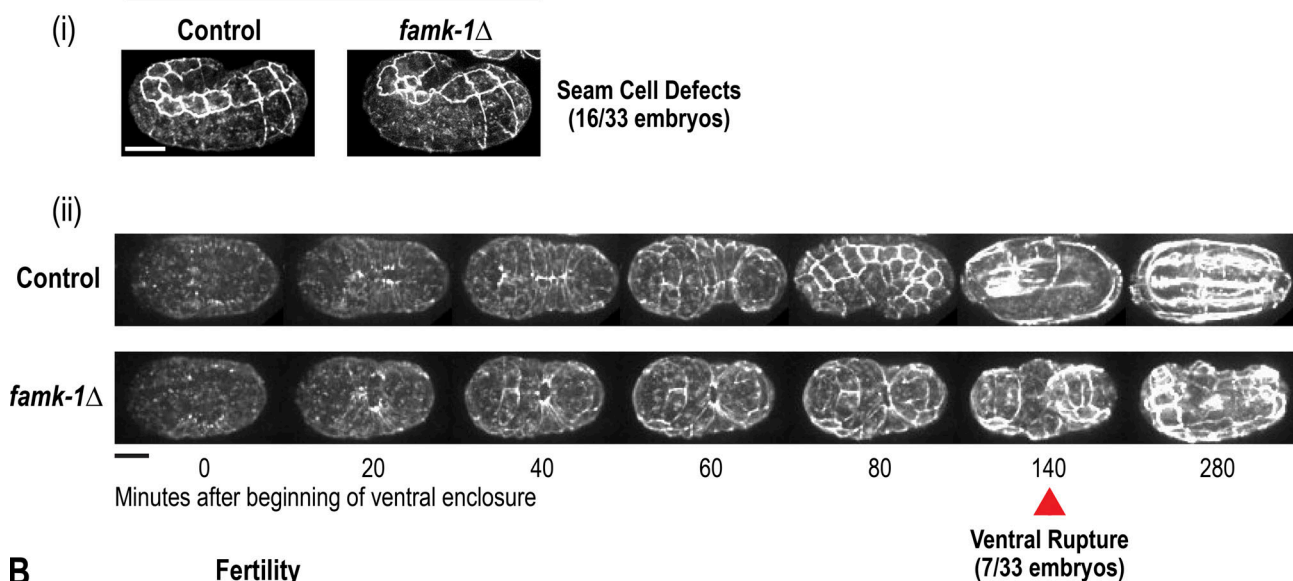
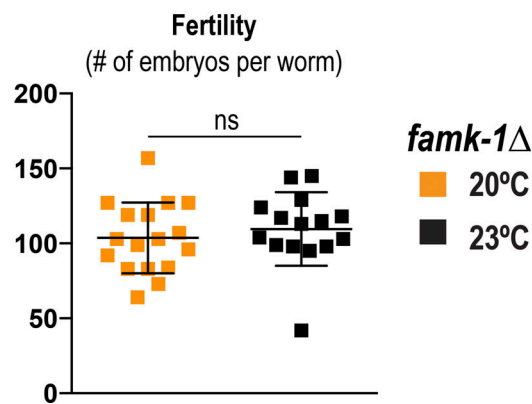
A**DLG-1::GFP****B**

Figure S3. **Analysis of DLG-1 localization and *famk-1Δ* fertility.** (A) Imaging of DLG-1::GFP in late-stage control and *famk-1Δ* embryos. Scale bars, 10 μ m. (B) Analysis of *famk-1Δ* fertility at 20°C and 23°C.

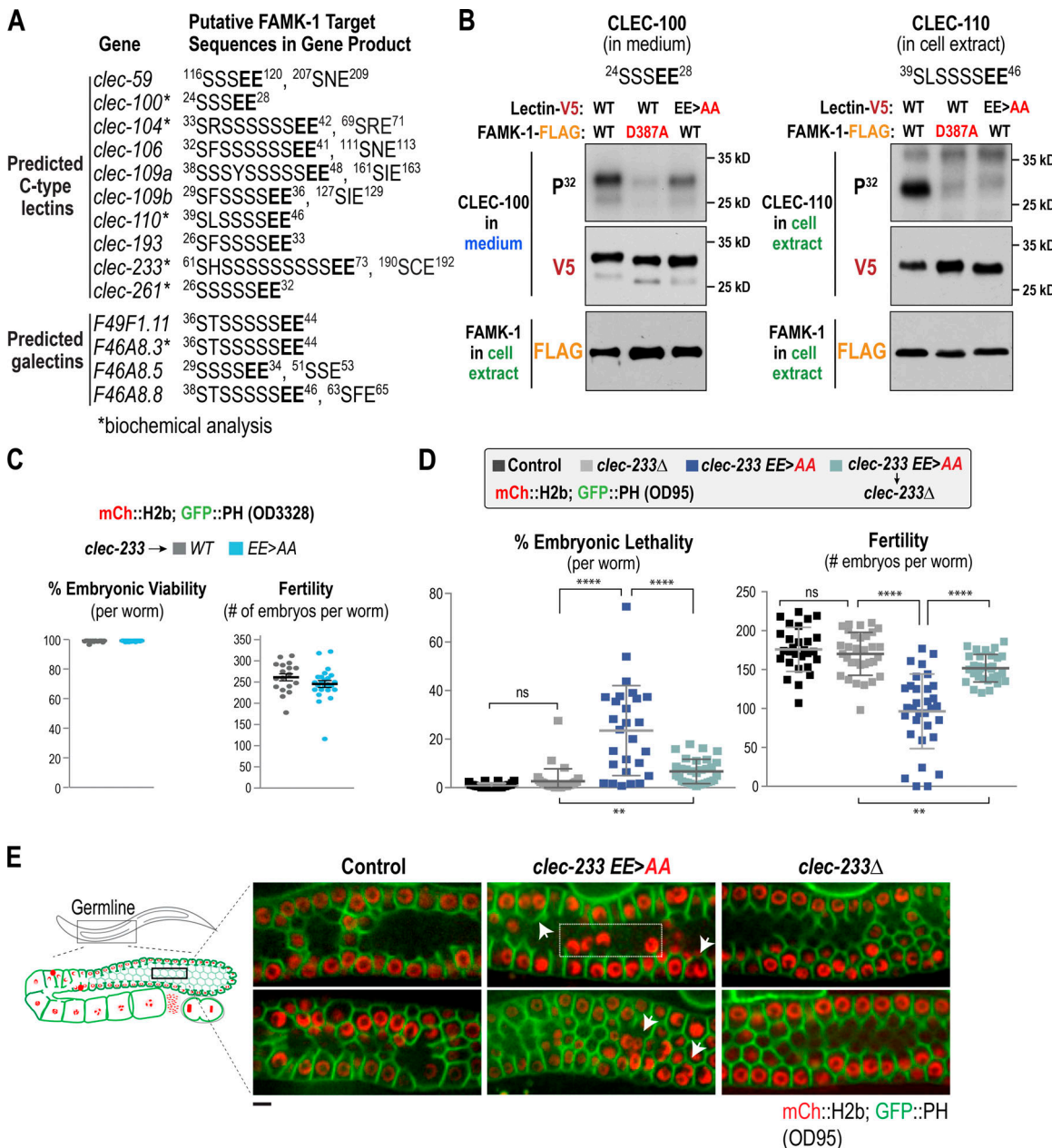


Figure S4. Analysis of lectins as putative substrates of FAMK-1. **(A)** Motifs identified by the proteome-wide search for SSSEE motifs. Additional “SxE” motifs in the same target are also listed. Residue numbers are indicated to identify location within the primary sequence. The products of genes marked with asterisks were subjected to biochemical analysis after coexpression with FAMK-1 in HEK293 cells (see Fig. 4 B). **(B)** Analysis of CLEC-100 and CLEC-110 phosphorylation by FAMK-1. CLEC-110 was not efficiently secreted, and thus, its phosphorylation status was analyzed in cell extracts rather than in the medium. **(C)** Embryo viability and fertility analysis in the presence of a single-copy targeted transgene expressing GFP::PH and mCh::H2b from strain OD3328. Unlike in the presence of transgenes derived from strain OD95 (two transgenes integrated by biolistic transformation, likely multicopy), the *clec-233*(EE>AA) mutant does not show appreciably reduced embryonic viability or fertility in this background. Error bars are the SEM. **(D)** Embryo viability and fertility analysis confirming that the reduced embryonic viability and fertility observed for the *clec-233*(EE>AA) mutant in the background of transgene insertions from OD95 is due to the engineered double glutamate-to-alanine mutation in *clec-233*. Error bars are the SD. ****, P < 0.0001; **, P < 0.01; ns, not significant (t tests). **(E)** Images of the germline in control and *clec-233*(EE>AA) worms in the presence of transgenes from the OD95 background. Arrows highlight nuclei delaminating from the gonad surface. Arrowheads point to multi-nucleated compartments in the germline. The box highlights nuclei that delaminated from the germline surface and have fallen into the interior. Similar defects were observed in 3 out of 10 imaged *clec-233*(EE>AA) worms. Scale bar, 5 μm.

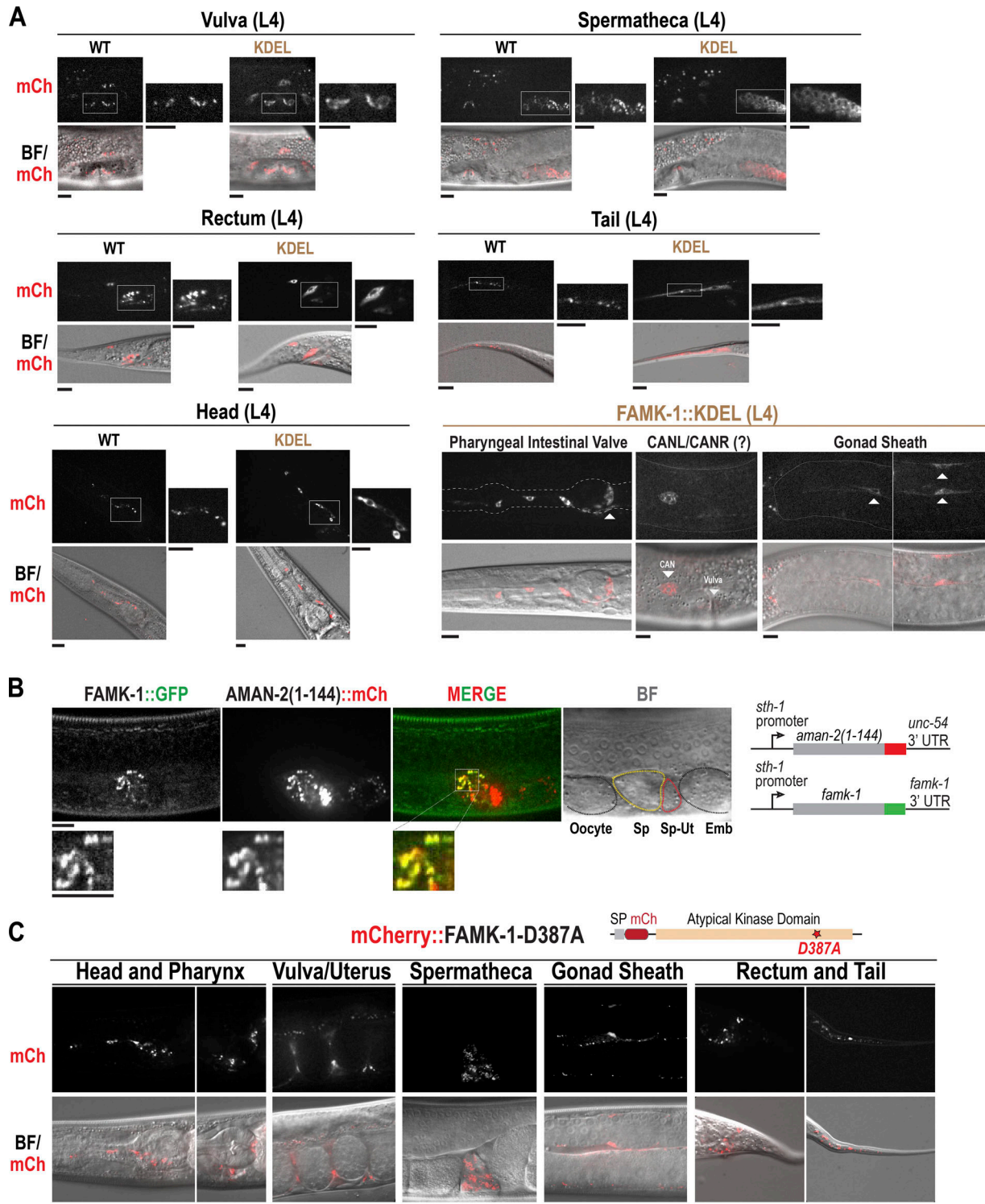


Figure S5. Analysis of WT and KDEL mCherry::FAMK-1 localization and FAMK-1 colocalization with a Golgi marker in spermatheca. (A) mCherry signal alone and overlay of bright-field (BF) and mCherry signals for WT and KDEL FAMK-1 in the indicated tissues. Representative images and magnified images of boxed regions are shown for each tissue; at least six worms were imaged per tissue. Scale bars, 10 μ m. (B) Analysis of FAMK-1::GFP and AMAN-2(1-144)::mCh colocalization; schematics on the right indicate the single-copy transgenes used for this analysis. The bright puncta of FAMK-1 in the spermatheca colocalized with Golgi-localized AMAN-2. The AMAN-2 fragment is also highly expressed in the spermatheca-uterine valve, potentially due to the distinct 3' UTR used in the *aman-2(1-144)::mCh* transgene. Scale bars, 10 μ m. (C) Localization of FAMK-1(D387A) kinase-defective mutant, tagged at its N-terminus after the signal sequence, in different tissues. Scale bar, 10 μ m.

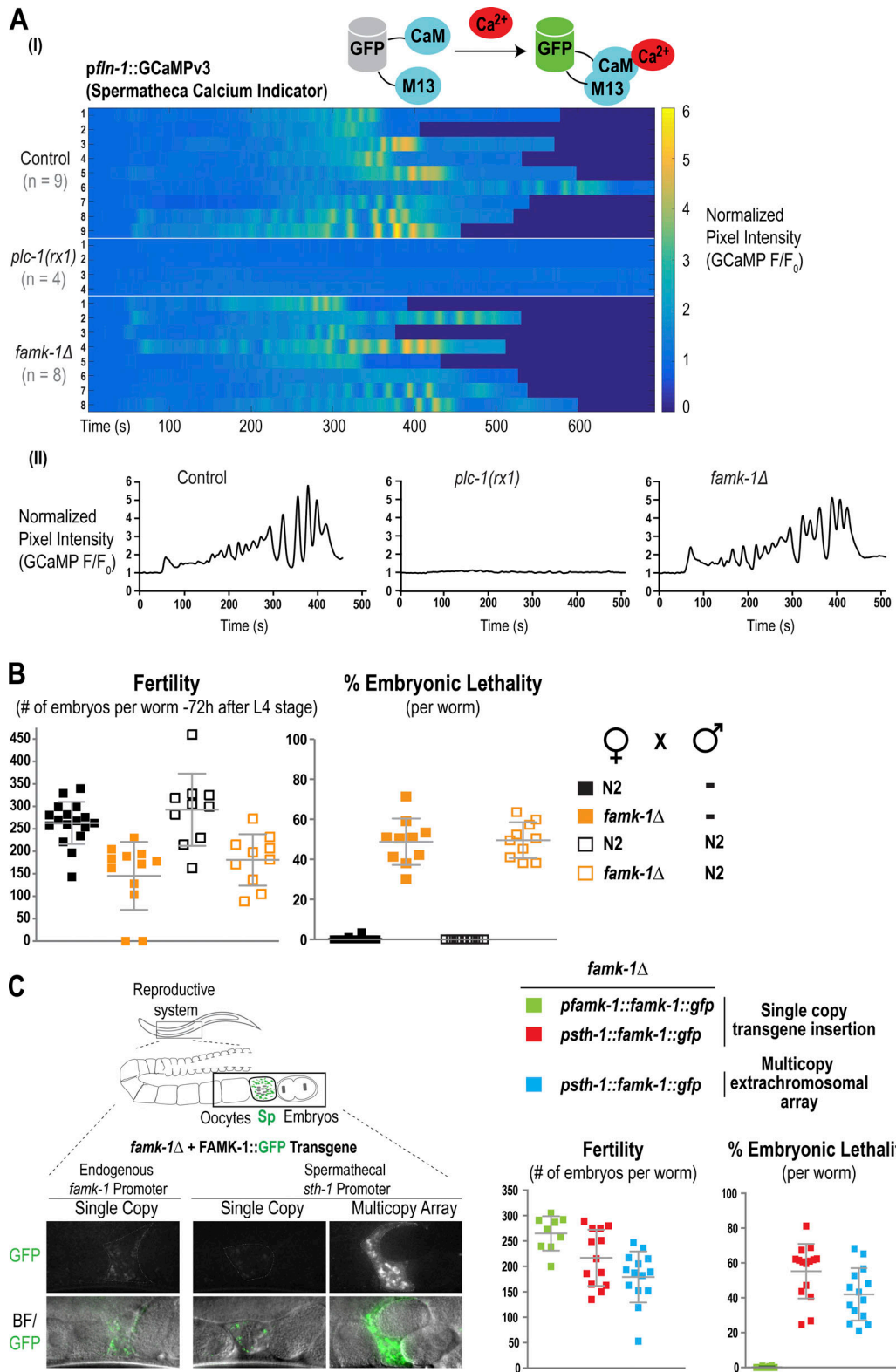
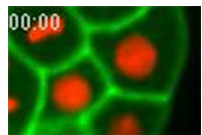


Figure S6. Analysis of spermatheca-expressed FAMK-1. (A) Analysis of calcium oscillations in the spermatheca using *pfln-1::GCaMPv3* during the first few ovulations of *C. elegans*. Each row represents an individual imaged worm. *plc-1(rx1)* serves as a positive control in that calcium oscillations are not observed in the spermatheca in this mutant. Plots below show the normalized pixel intensity for representative individual worms. (B) Mating with N2 males does not restore the fertility or embryo viability of *famk-1Δ*. Successful mating was confirmed by presence of males among the F1 progeny. (C) Left: Images of FAMK-1::GFP expressed under control of the spermathecal promoter *psth-1* (single copy or multicopy array) or under control of the endogenous promoter, *pfln-1* (single copy). Overlay images of bright-field (BF) and GFP signal images are shown below. Scale bar, 20 μ m. Right: Effect of overexpression of FAMK-1 from an extrachromosomal array on fertility and embryonic viability at 20°C.

Provided online are three tables in Excel. Table S1 lists hits from proteome-wide “SSSEE” motif search, which are predicted to also have a signal peptide and/or transmembrane domains. Table S2 lists *C. elegans* strains used in the study. Table S3 lists plasmids used for analysis of FAMK-1 substrate phosphorylation.



Video 1. Example of partition loss between adjacent cells resulting in multinucleation in a *famk-1Δ* embryo. Frames were acquired every 20s. Playback is at 2 frames per second.